JACS
JOURNAL OF THE AMERICAN CHEMICAL SOCIETY

Article

pubs.acs.org/JACS

Organelle-Specific Detection of Phosphatase Activities with Two-Photon Fluorogenic Probes in Cells and Tissues

Lin Li, Jingyan Ge, Hao Wu, Qing-Hua Xu, and Shao Q. Yao*

Department of Chemistry, National University of Singapore, Singapore 117543

Supporting Information

ABSTRACT: Two-photon fluorescence microscopy (TPFM) provides key advantages over conventional fluorescence imaging techniques, namely, increased penetration depth, lower tissue autofluorescence and self-absorption, and reduced photodamage and photobleaching and therefore is particularly useful for imaging deep tissues and animals. Enzyme-detecting, small molecule probes provide powerful alternatives over conventional fluorescent protein (FP)-based methods in bioimaging, primarily due to their favorable photophysical properties, cell permeability, and chemical tractability. In this article, we report the first fluorogenic, small molecule reporter system (**Y2**/**Y1**) capable of imaging endogenous phosphatase activities in both live mammalian cells and Drosophila brains. The one- and two-photon excited photophysical properties of the system were thoroughly investigated, thus confirming the system was indeed a suitable Turn-ON fluorescence pair for TPFM. To our knowledge, this is the first enzyme reporting two-photon fluorescence bioimaging system which was designed exclusively from a centrosymmetric dye possessing desirable two-photon properties. By conjugation of our reporter system to different cell-penetrating peptides (CPPs), we were able to achieve organelle- and tumor cell-specific imaging of phosphatase activities with good spatial and temporal resolution. The diffusion problem typically associated with most small molecule imaging probes was effectively abrogated. We further demonstrated this novel two-photon system could be used for imaging endogenous phosphatase activities in Drosophila brains with a detection depth of >100 μm.

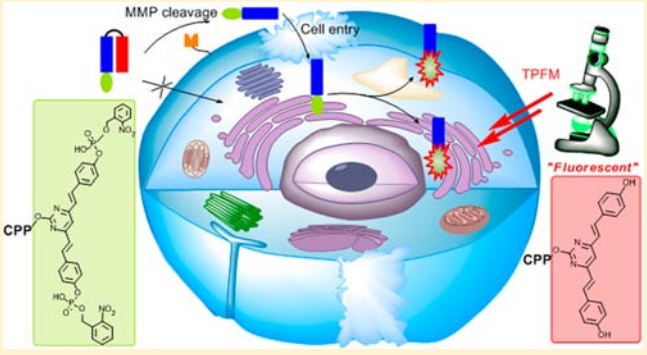

INTRODUCTION

Phosphatases are a large and structurally diverse class of signaling enzymes that remove the phosphate group from their protein and nonprotein substrates. Defective regulation of these enzymes has significant implications in human diseases.[1] Of the various types of phosphatases, protein phosphatases (PPs) are the most common and important as they control the reversible phosphorylation/dephosphorylation process in up to 30% of all human proteins. There are two major classes of PPs, namely protein tyrosine phosphatases (PTPs) and serine/threonine phosphatases. It is well documented that elevated levels of endogenous PP activities (especially those of PTPs) are associated with tumorigenesis in numerous cells and tissues.[2] Acid and alkaline phosphatases (abbreviated as ACPs and ALPs, respectively) are the other two types of phosphatases that are present in most human organs and tissues, and their levels of expression have been routinely used for disease diagnosis.[3,4] For example, the serum level of certain ACPs is used to evaluate the success of the surgical treatment of prostate cancer.[3] Since ALP is a byproduct of osteoblast activity, elevated ALP has been used to diagnose bond-forming diseases such as Paget's disease.[4a] The ALP found within white blood cells, commonly referred to as Leukocyte alkaline phosphatase (LAP), is used in diagnosis of conditions such as polycythemia vera, primary myelofibrosis, and chronic/accute chronic myelogenous leukemia.[4b] Consequently, biological and chemical approaches capable of reporting phosphatase expression, and more importantly their activities, would provide invaluable insights into how these enzymes work under physiological settings and how they could be modulated therapeutically.[5−8] Of particular significance are probes suitable for live-cell and deep-tissue imaging.[9,10] Existing methods in phosphatase biology, such as those based on gene knockout or overexpression techniques, do not provide an adequate view of the temporal, spatial, and dynamic properties of phosphatases in cells.[5] Emerging tools have begun to address some of these issues by focusing on the detection of phosphatase activities at the proteome level or in living cells.[6−8] Among them, imaging-based approaches are highly desirable due to their high sensitivity and good resolution.[9] Bastiaen and co-workers developed the first PTP imaging approach based on Förster resonance energy transfer (FRET).[7] The method relies on spatial resolution of the enzyme−substrate (ES) interaction between a PTP genetically fused to a fluorescent protein (FP) donor and a dye-labeled, synthetic phosphopeptide acceptor,

Received: April 16, 2012
Published: June 26, 2012

   dx.doi.org/10.1021/ja3036256 | J. Am. Chem. Soc. 2012, 134, 12157−12167

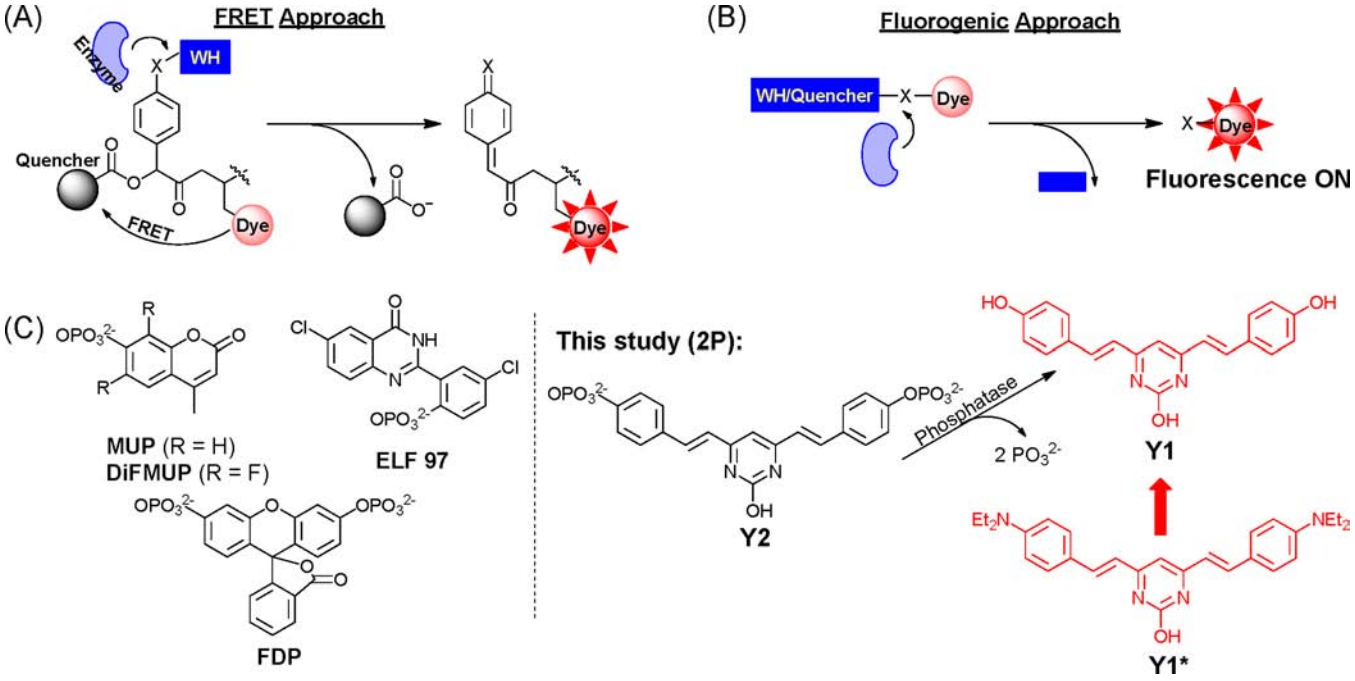

Figure 1. Two practical strategies for generation of two-photon, enzyme-detecting small molecule probes. (A) The FRET-based strategy recently developed in our previously work.[17] (B) The two-photon fluorogenic approach presented in the current study, which necessitates the discovery of a centrosymmetric dye with detectable two-photon excited fluorescence. (C) Commercially available 1P fluorogenic phosphatase reporters (left), all of which have undesirable 2P properties, and the 2P fluorogenic phosphatase reporter developed in the current study (**Y2**; right). Upon removal of the phosphate groups in **Y2** by a phosphatase, the highly fluorescent **Y1**, which possesses good 2P photophysical properties, is generated. **Y1** was designed based on a previously known 2P centrosymmetric dye, **Y1***.[19]

and therefore was able to indirectly monitor PTP activities in cells. The need to deliver the peptide into cells by microinjection, however, makes this strategy technically demanding. A genetically encoded calcineurin (a serine/threonine phosphatase) biosensor was recently reported,[8] but similarly to other macromolecular imaging probes based on FRET and protein conformation changes, it offers limited utilities as a general phosphatase imaging probe.[11] Small molecule-based probes provide a powerful tool for live-cell and tissue imaging, primarily due to their desirable properties, including permeability (due to their small sizes), photophysical properties (e.g., good photo stability), chemical tractability (e.g., different molecular structures/designs can be installed), and amenability to a wide variety of biological events.[10] Of the various types of small molecule probes, those capable of detecting enzymatic activities (either *in vitro* or *in situ*) are typically designed based on either the FRET (Figure 1A) or the fluorogenic approach (Figure 1B), but most of them can readily diffuse away from the site of the enzymatic reaction *in situ*, thus providing limited utilities for subcellular imaging.[12] Several fluorogenic substrates of phosphatases, which are based on well-known small organic fluorophores such as coumarin, fluorescein, and their analogues, are available (Figure 1C; left), and have been widely used *in vitro* for general phosphatase detection.[13] These phosphatase probes, due the presence of the negatively charged phosphate group in the reporters, are not cell-permeable, but may be made so by "caging" the phosphate with a removable 2-nitrobenzyl protecting group.[14] Some of them have even been developed into magnetic resonance Imaging (MRI)-based agents for detection of ALP activities in bone tissues.[15] Notwithstanding, the diffusible nature of these small molecule probes still poses a serious challenge for cell-based imaging where sufficient spatial resolutions are needed.[12]

The commercially available product ELF 97 provides one such exception (Figure 1C; left). Upon enzymatic removal of the phosphate group, the compound forms a bright yellow-green fluorescent precipitate at the site of reaction and thus is able to detect phosphatase activities in cells with sufficient spatial resolution. ELF 97, however, is not cell-permeable and therefore can only be used *in vitro* or in fixed cells. Innovative designs in several newly emerging, enzyme-detecting small molecule probes have begun to address this diffusion problem.[16−18] Bogyo and co-workers recently developed quenched activity-based probes (*q*ABPs) to monitor real-time protease activities in live human cells. By using acyloxymethyl ketone (AOMK)-based probes which emit a strong fluorescent signal only after proteolysis by a cysteine protease target, with the simultaneous formation of a covalent probe enzyme adduct, this strategy couples imaging and self-immobilization within the same design to achieve the intended "Turn-ON" imaging capability for cysteine proteases *in vivo* with good spatial resolution.[16] The design, however, was not easily amenable to imaging most other types of enzymatic activities (e.g., phosphatases). On the basis of a similar concept, we recently developed the first small molecule probe capable of detecting endogenous phosphatase activities with acceptable spatial resolution in live cells (Figure 1A);[17] our method incorporated a quinone methide system into the FRET-based approach (Figure 1A) with a two-photon (2P) dye, 2-hydroxy-4,6-bis(4-(diethylamino)styryl)pyrimidine (**Y1***; Figure 1C; right),[19] and a quencher, 4-(4-dimethylaminophenyl)diazenylbenzoic acid (Dabcyl). Upon enzymatic phosphate removal, the quencher was released from the probe, and at the same time a highly reactive quinone methide intermediate was generated which subsequently "fixed" the fluorescent adduct near the site of the reaction, thus achieving good spatial resolution. The need for

dx.doi.org/10.1021/ja3036256 | J. Am. Chem. Soc. 2012, 134, 12157−12167

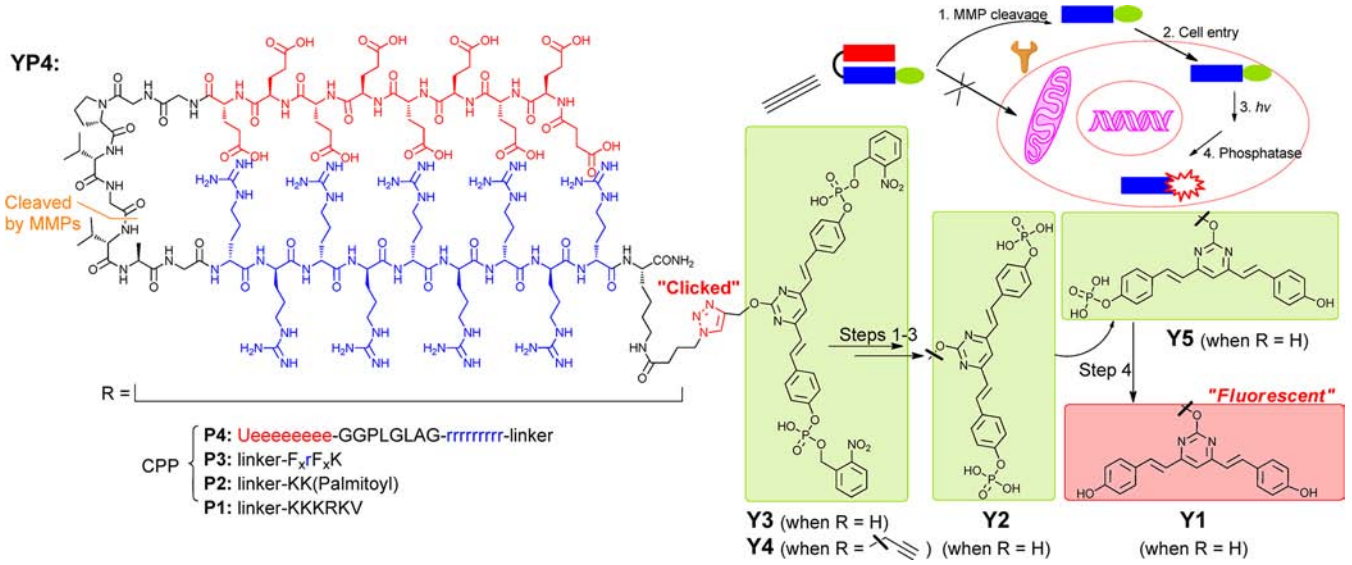

Figure 2. Overall strategy of the four CPP-conjugated 2P fluorogenic substrates, **YP1** to **YP4**. They were used for subcellular bioimaging of endogenous phosphatase activities in mammalian cells and Drosophila brains. The 2P reporter in all four conjugates was in the "caged" form (similar to **Y3**, where R = H). Sequences of the four CPPs (**P1** to **P4**) were shown by their single-letter amino acid alphabets. Unnatural AAs were represented as F_x = *L*-cyclohexylalanine; r = *D*-Arg; e = *D*-Glu; U = succinic acid. The full structure of **YP4** is shown, with the negatively charged *D*-Glu/succinic acid and the positively charged *D*-Arg highlighted in red and blue, respectively. MMP cleavage site in **YP4** is indicated. In the tumor cell-specific approach, membrane-bound MMPs first cleaved the masking "red" peptide fragment (Step 1), exposing the "blue" CPP and delivering the probe into the cells (Step 2). Subsequent UV irradiation (Step 3) released the phosphatase-responsive probe **Y2**, which was dephosphorylated by endogenous PPs, generating highly fluorescent and localized **Y1** (Step 4), possibly through the monophosphorylated intermediate **Y5**.

introducing the Dabcyl group, however, made the resulting probe significantly bulkier than needed and rendered it cell-impermeant.

Two-photon (2P) fluorescence microscopy (TPFM) provides key advantages over conventional one-photon (1P) imaging techniques, namely, increased penetration depth, lower tissue autofluorescence and self-absorption, reduced photodamage and photobleaching, and therefore is particularly useful for imaging deep tissues and animals.[9,20,21] Various reactive 2P probes have been developed for metal cations, organic and inorganic anions, DNA and other targets.[21] Practical 2P small molecule probes (that is, probes made of fluorescent dyes that possess desirable 2P photophysical properties) capable of detecting endogenous enzyme activities, to our knowledge, are unavailable at present, apart from our most recent report.[17] In principle, a "piggyback" approach may be taken by using some of the existing 1P probes (e.g., the coumarin and fluorescein probes shown in Figure 1C) in a 2P experiment.[20] This, however, has not been very successful, primarily due to undesirable 2P photochemical and photophysical properties of coumarin and fluorescein dyes. For TPFM to be widely adopted for bioimaging of enzymatic activities, it is essential that fluorogenic enzyme substrates based on novel 2P dyes are developed.[10,20] Inspired by our recent work of the FRET-based 2P probe, we reasoned that **Y1*** and other similarly designed 2P dyes having the same core structure (e.g., 2-hydroxy-4,6-bis(4-hydroxystyryl)pyrimidine, or **Y1**, in Figure 1C, right) might indeed be made into fluorogenic dyes/reporters. A well-known strategy to turn ON/OFF a dye is to change the pull–push conjugated π-electron system within the dye. This principle had previously been successfully applied in the development of fluorogenic probes based on coumarin and fluorescein dyes (Figure 1C; left).[22] As part of the current study, we found that fluorescence of the newly developed 2P dye, **Y1** (Figure 1C right; via $NR_2 \rightarrow OH$ conversion from the previously reported 2P dye, **Y1***), upon attachment of an electron-withdrawing phosphate group (giving **Y2**; Figure 1C, right), was effectively turned OFF in aqueous buffers. This thus makes **Y1**, to our knowledge, the first fluorogenic reporter developed from a centrosymmetric dye possessing desirable 2P photophysical properties. Herein, we report the successful demonstration of **Y1**, and the resulting probes based on it, as efficient Turn-ON 2P imaging reporters for detection of endogenous phosphatase activities with good spatial resolution in both cells and tissues.

RESULTS AND DISCUSSION

Design of the Two-Photon Fluorogenic Probes. In our approach (Figure 2), **Y1** serves as the 2P fluorescence reporter. Its phosphorylated version **Y2**, where the two phenolic groups were masked by an electron-withdrawing, phosphatase-responsive phosphate warhead, has a significantly reduced conjugated π-electron system, and thereby represents the Turn-OFF state of **Y1**. **Y3**, the "caged" form of **Y2**, which releases the active phosphatase reporter upon UV irradiation, increases the cell permeability of the reporter and at the same time provides additional spatial and temporal controls over imaging endogenous phosphatase activities.[14,17] In the current study, we chose a simple photolabile 2-nitrobenzyloxy group as the caging molecule for synthetic convenience, but it may be readily replaced, if necessary, with other known two-photon caging molecules.[21d,e] To minimize the diffusion problem of our probes while imaging endogenous phosphatase activities and to make them suitable for subcellular detection of localized enzymatic activities in live cells, we conjugated **Y4**, which is an alkyne-containing analog of **Y3** (Supporting Information, Scheme S1), to different azide-modified, cell-penetrating peptides (CPPs; **P1** to **P4** in Figure 2 and Scheme S1), giving **YP1**/**YP2**/**YP3**/**YP4** (Figure 2 and Scheme S1). We chose the Cu(I)-catalyzed cycloaddition, or click chemistry, for highly

dx.doi.org/10.1021/ja3036256 | J. Am. Chem. Soc. 2012, 134, 12157–12167

modular and rapid assembly of these small molecule probe–peptide conjugates, which would have otherwise been challenging to obtain synthetically.[23] Of the four CPPs chosen, **P1** is a peptide derived from Simian virus 40 (SV40) T-antigen.[24a] The resulting **P1**-conjugated probe, **YP1**, was expected to be delivered to the endoplasmic reticulum (ER) of mammalian cells and detect ER-localized phosphatase activities therein. **YP2**, conjugated to the *N*-palmitoylated plasma membrane localization peptide **P2** which is commonly found on membrane-bound proteins,[24b] would detect membrane-localized phosphatase activities. **YP3** (conjugated to a well-known mitochondria-localizing peptide, **P3**, developed by Kelley et al.[24c]) would detect mitochondria-localized phosphatase activities. To investigate whether our strategy could also be used to image endogenous phosphatase activities in a tumor cell-specific manner, we designed **YP4**, which is conjugated to the **P4** peptide. The **P4** peptide contains a polycationic CPP peptide (in blue) fused to a polyanionic masking peptide (in red) through a linker cleavable by matrix metalloproteases (MMPs) which are overexpressed on the surface of numerous cancer cells including HeLa cells. Previously, Tsien and co-workers had successfully used this peptide as a vehicle for tumor cell-specific delivery.[25] As shown in Figure 2, cellular uptake of **YP4** would normally be blocked due to the charge interaction between the two peptide fragments, but upon cleavage by MMPs present on tumor cells (Step 1), the CPP peptide would be locally unleashed, causing the cleaved **YP4** to be internalized to the intended subcellular organelle (i.e., ER; Step 2). Subsequent UV irradiation (Step 3) would release the phosphatase-responsive probe **Y2** (still conjugated to the peptide), which would then be dephosphorylated by endogenous phosphatases, generating the highly fluorescent and localized **Y1** (Step 4).

Chemical Synthesis. Synthesis of the newly discovered 2P fluorogenic dye, 2-hydroxy-4,6-bis(4-hydroxystyryl)pyrimidine, **Y1**, its phosphorylated **Y2** and the "caged" version **Y3** is shown in Scheme S1 (Supporting Information). The compounds were synthesized according to previously published protocols with some modifications.[19] Briefly, 2-hydroxy-4,6-dimethylpyrimidine (**1**) was condensed with 2.2 equivalents of 4-hydroxybenzaldehyde in the presence of hydrochloric acid under reflux conditions to give **Y1** in a single step (80% yield). Similarly, **Y2** was prepared from diethyl 4-formylphenyl phosphate (**2**) followed by TMSI deprotection in 15% yield (in two steps). The nitrobenzyl protected **Y3** was prepared by condensation between (**1**) and 4-aldehydephenyl bis(2-nitrobenzyl) phosphate (**3**) in 21% yield. The propargyl group-containing **Y4** was prepared by coupling propargyl bromide to **Y3** in the presence of K_2CO_3 (37.5% yield). **Y5** (used as a control in our studies), the monophosphorylated version of **Y2**, was synthesized by the coupling of (**1**) with 1.1 equiv of 4-hydroxybenzaldehyde, giving (*E*)-4-(4-hydroxystyryl)-6-methylpyrimidin-2-ol (**4**) (72% yield). The subsequent reaction between (**4**) and (**2**) followed by TMSI deprotection gave the desired product **Y5** in 11% yield (in two steps). The four azide-functionalized localization peptides were synthesized on rink amide resin using protocols modified from standard solid phase peptide synthesis (SPPS; Supporting Information, Scheme S1).[26] For **P1** and **P3**, the corresponding amino acids were assembled on the resin. At the end of the synthesis, 4-azidobutanoic acid was coupled to the resin using HOBt/HBTU/DIEA activation strategy. For **P2**, the palmitoyl group was first attached to Ω-amino group of the first Lys residue by HOBt/HBTU/DIEA coupling. Subsequent SPPS and the coupling of 4-azidobutanoic acid were similarly followed. For **P4**, since a succinic acid moiety was needed as the *N*-terminal cap of the peptide, 4-azidobutanoic acid was added to the Ω-amino group of the first Lys residue instead (Supporting Information, Scheme S1). The peptides were cleaved from the resin and purified by reverse-phase preparative HPLC to homogeneity and characterized by LC–MS. To obtain the peptide-reporter conjugates, **YP1**–**YP4**, a variety of "click" conditions were tested for the coupling between **Y4** and **P1**-**P4**; at the end, it was found a cosolvent system of DMSO/H_2O (1:1) with copper catalysts and additives ($CuSO_4$/NaAsc/TBTA) gave the best results for **YP1**/**YP2**/**YP3**, and for **YP4**, a cosolvent system of DMSO/CH_3CN/H_2O (4:4:1) with CuI/DIEA worked the best. All four conjugates were obtained in good coupling efficiency and product quality. They were similarly purified and characterized.

Photophysical and Enzymatic Properties of Probes. To unequivocally establish that our newly developed **Y1**/**Y2** pair was indeed a good 2P fluorogenic system capable of emitting strong fluorescence during **Y2**→**Y1** conversion and thus reporting phosphatase activities in real time, we next investigated their photophysical (1P and 2P) and enzymatic properties (Table 1, Figures 3 and 4; Figures S1–S3 in the Supporting Information). **Y3** (the "caged" version of **Y2**), **Y5** (the monophosphorylated version of **Y1**) as well as two common 1P dyes, coumarin and fluorescein, were included in the experiments as references. As shown in Table 1, under physiological conditions (Hepes buffer at pH = 7.5), **Y1**/**Y2**/**Y3**/**Y5** had maximum absorption spectra at 400–420 nm,

Table 1. Photophysical Properties of Y1/Y2/Y3/Y5

	$\lambda_{max}^{(ab)a}$	$\varepsilon/10^3$	$\lambda_{max}^{(em)b}$	$\varepsilon\Phi^c$	τ^d	$\delta\Phi^e$
Y1	421	49	512	5390	0.340	82
Y2	406	28	532	1960	0.315	21
Y3	404	18	481	1620	0.320	25
Y5	405	33	522	3300	0.325	39

[a]Peak position of the longest absorption band. [b]Peak position of emission, exited at the absorption maxima in Hepes. [c]Brightness of the relative compound. [d]Life time of the emission in ns. [e]The maximum two-photon action cross-section values upon excitation from 750 to 860 nm in GM (1 GM = 10^{-50} cm^4 s $photon^{-1}$).

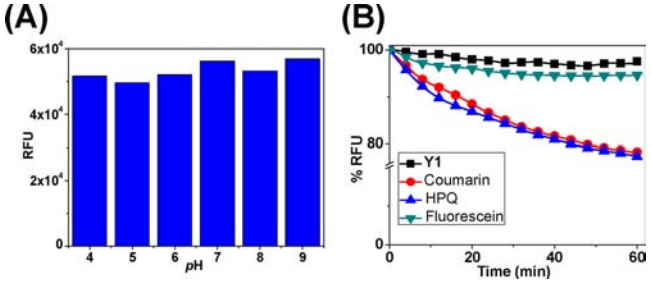

Figure 3. (A) pH Effect on the one-photon excited fluorescence intensity of **Y1** at room temperature in Hepes buffer (supplemented with 50 mM NaCl, 2.5 mM EDTA, 2 mM DTT and 0.02% Triton X-100; probe concentration: 1.0 μM; $\lambda_{ex/em}$ = 405/550 nm). (B) Photostability profiles of **Y1** and three commercial dyes (coumarin, HPQ, and fluorescein) over the course of 60 min in Hepes buffer ($\lambda_{ex/em}$ = 405/550 nm for **Y1**, 350/450 nm for courmarin, 350/520 nm for HPQ, and 488/520 nm for fluorescein).

dx.doi.org/10.1021/ja3036256 | J. Am. Chem. Soc. 2012, 134, 12157–12167

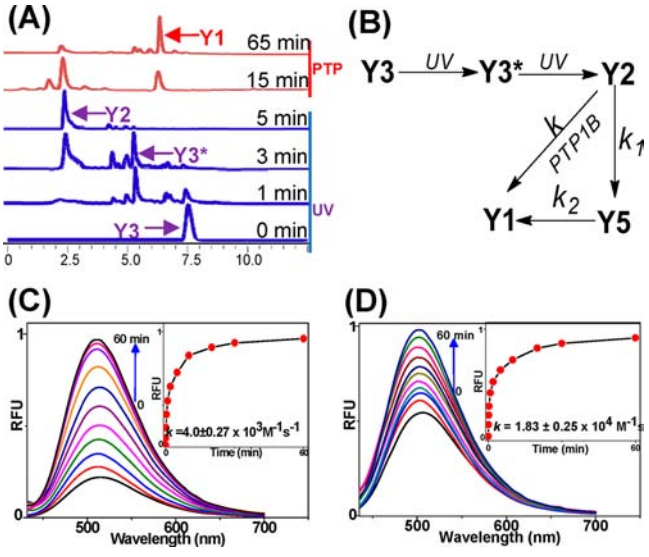

Figure 4. (A) **Y3**→**Y2** conversion by UV irradiation (5 min), followed by **Y2**→**Y1** dephosphorylation by PTP1B (60 min). Reactions were carried out at room temperature in Hepes buffer (supplemented with 50 mM NaCl, 2.5 mM EDTA, 2 mM DTT and 0.02% Triton X-100, *p*H = 7.5; probe concentration: 1.6 μM). Experiments were monitored by LC−MS, and peaks were unambiguously assigned based on their molecular weights. PTP1B/probe concentration ratio = 1:30. **Y5** was not detected throughout the entire **Y2**→**Y1** process. (B) Overall pathway of **Y3**→**Y2**→**Y1**. (C,D) Time-dependent one-photon excited fluorescence emission spectra of PTP1B-treated **Y2** and **Y5** reactions, respectively, over the course of 60 min.

making them suitable to be excited by a common two-photon laser. **Y1** had a fluorescence maximum at λ_{em} = 512 nm (ε = 49000 M^{-1} cm^{-1} and $\varepsilon\cdot\Phi$ = 5390) which was largely independent of *p*H changes (Figure 3A), and a two-photon action cross-section ($\delta\cdot\Phi$ = 82 GM) comparable to other common 2P dyes.[21] On the contrary, **Y2** and **Y3** were only weakly fluorescent ($\varepsilon\cdot\Phi$ = 1960 and 1620, respectively) and had much smaller two-photon action cross sections ($\delta\cdot\Phi$ = 21 and 25 GM, respectively). **Y5**, with an absorption maximum at λ_{ab} = 405 nm and fluorescence emission maximum at λ_{em} = 522 nm (ε = 33000 $M^{-1}cm^{-1}$, $\varepsilon\cdot\Phi$ = 3300, $\delta\cdot\Phi$ = 39 GM), was moderately fluorescent as well, due to removal of one of the phosphate groups in **Y2**. **Y1** showed excellent photostability which was better than courmarin, fluorescein, and 2-(2′-hydroxy-5′-chlorophenyl)-6-chloro-4-(3*H*)-quinazolinone (HPQ) (Figure 3B). The consistent fluorescence lifetime (τ) in the **Y1**/**Y2** system indicates the fluorogenicity of the system was based on the increase in the absorbance during **Y2**→**Y1** conversion, which is similar to other well-known fluorogenic phosphatase reporter systems (e.g., DiFMUP, MUP, ELF-97, and FDP in Figure 1C).[22] Unlike **Y2**, both **Y1** and **Y3** were shown to be highly cell-permeable (P_{app} = 223 and 233 nm·s^{-1}, respectively). We therefore concluded that the **Y1**/**Y2**/**Y3** system was suitable for endogenous phosphatase imaging using TPFM.

Next, it was established that a completely uncaged product **Y2** could be obtained from **Y3** (through its monoprotected intermediate **Y3*** which was detectable by HPLC) under UV exposure of 500 μJ/cm^2 for 5 min (Figure 4A). Further incubation of the uncaged **Y3** with PTP1B (a key human PTP involved in diabetes and obesity),[27a] and other types of phosphatases (Figure S3; including alkaline phosphatase from bovine intestinal mucosa, two human serine/threonine phosphatases, PP1 and PP2B, which are involved in cell division and T cell activation, respectively[27b,c]) gave rise to almost complete **Y2**→**Y1** conversion in 60 min, with a concomitant increase in fluorescence (Figure 4C). With the presence of two phosphate groups in the molecule, **Y2** might have been first dephosphorylated to **Y5** *on route* to **Y1** (Figures 2 and 4B), and if so, it might potentially complicate the real-time reporting of phosphatase activities. We were pleased to find, however, that the formation of **Y5** was not detected in our LC−MS experiments throughout the duration of **Y2**→**Y1** process (Figure 4A). This indicates a faster rate of **Y5**→**Y1** (k_2) than that of **Y2**→**Y5** (k_1) as illustrated in Figure 4B. As such, with **Y2**→**Y5** being the rate-determining step, readouts from the fluorescence increase of **Y2** upon phosphatase treatment should accurately reflect the overall rate of **Y2**→**Y1** (k). Subsequently, time-dependent fluorescence measurements were carried out with PTP1B-treated reactions (**Y2** in Figure 4C and **Y5** in Figure 4D), and the results were extrapolated to provide the corresponding kinetic parameters. On the basis of the reaction model shown in Figure 4B, we obtained reaction rate constants of $k = 4.00 \pm 0.27 \times 10^3$ M^{-1} s^{-1} and $k_2 = 1.83 \pm 0.25 \times 10^4$ M^{-1} s^{-1}. These results thus corroborated well with our earlier LC−MS results (Figure 4A).

Subcellular Bioimaging of Endogenous Phosphatase Activities with YP1/YP2/YP3. We first established that our newly developed **Y1**/**Y2**/**Y3** fluorogenic system was indeed useful for general bioimaging applications to detect endogenous phosphatase activities. Since **Y3** (the "caged"version of **Y2**) is cell-permeable, it was used in our preliminary imaging experiments (Figure 5). The ELF 97 detection kit was used as a control to detect endogenous phosphatase activities in fixed mammalian cells (Supporting Information, Figure S4);[13a] fluorescence signals were detected mostly throughout the whole cell (except nucleus), indicating the ubiquitous presence of phosphatase activities across most intracellular space and organelles. Real-time imaging of live HepG2 cells treated with the cell-permeable **Y3** probe, upon UV irradiation (to give intracellular **Y2**), showed a gradual increase in fluorescence signals in the whole cell (similar to ELF 97) over the course of 60 min. After 60 min, the fluorescence reached saturation

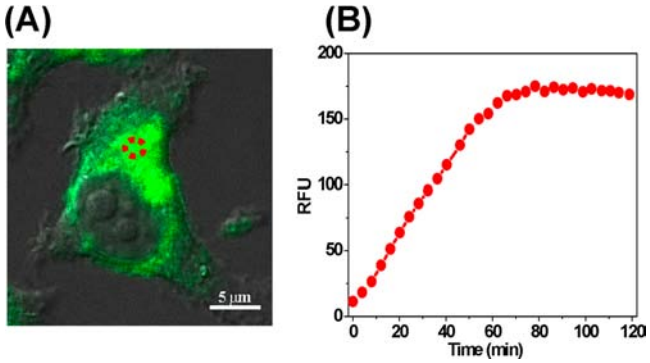

Figure 5. (A) One-photon excited fluorescence microscopy of live HepG2 cells treated with **Y3** (10 μM). Following 2-min UV irradiation, the cells were imaged over the course of 120 min with 60-s intervals (λ_{ex} = 405 nm; PMT range: 460−550 nm). The image shown was taken at the 80-min time point. Scale bar = 5 μm. (B) Graphical representation of time-dependent changes in fluorescence intensity at the circled position in panel A.

dx.doi.org/10.1021/ja3036256 | *J. Am. Chem. Soc.* 2012, 134, 12157−12167

(Figure 5). This kinetic profile was similar to what was observed in the *in vitro* experiment with recombinant PTP1B (Figure 4C). We thus concluded **Y3** alone could be used to detect endogenous phosphatase activities with similar kinetic profiles as those from *in vitro* experiments. We further confirmed that the short UV irradiation conditions used in our imaging experiments did not cause any apparent changes in cell morphology and viability, as well as endogenous phosphatase activities (Supporting Information, Figure S5).

We next investigated whether the probes could be successfully delivered to subcellular organelles in live mammalian cells, for the maging of phosphatase activities localized therein. Direct administration of **Y3** to cells followed by UV irradiation/imaging, as shown in Figure 5, was not expected to provide sufficient spatial resolutions needed for subcellular imaging due to the diffusible nature of this compound. We therefore conjugated the probe to various cell-penetrating peptides (CPPs), giving **YP1**/**YP2**/**YP3** (Supporting Information, Scheme 1 Figure 2). Subcellular targeting was previously demonstrated for inhibitors and probes in cultured cells, using delivery vehicles including small molecules, localized CPPs and SNAP-tag fusion proteins.[26a,28] The use of localization peptides as delivery tools offers the advantages of better controlled administration, ease of synthesis and organelle specificity.[28c] Subcellular imaging of endogenous metabolites aided by small molecules or proteins has also been demonstrated recently.[24c,28b] Our aim in the current study was for the CPPs to achieve both organelle-specific delivery and subcellular retention of the probes, thus ensuring the released fluorescence be spatially imaged with sufficient resolutions. HeLa cells incubated with control dye-CPP conjugates indicated expected organelle-specific localization for all CPPs tested (Supporting Information, Figure S6). Subsequently, the imaging of endogenous phosphatase activities was carried out with both one- and two-photon fluorescence microscopy in live HeLa and HepG2 cancer cells (Supporting Information, Figure S7 and Figure 6). To image subcellular phosphatase activities using the CPP-conjugated probes, live cells were first incubated with the corresponding compound, irradiated by UV then imaged using TPFM (excitation at 800 nm; Figure 6). All three probes (**YP1**, **YP2**, and **YP3**) showed strong fluorescence signals ONLY in their intended organelles (ER, membrane and mitochondria, respectively), but not in other subcellular organelles and intracellular space (see image panels 3/7/11 in Figure 6). The same cells were simultaneously treated with commercially available organelle-specific imaging markers to independently verify the results (see image panels 2/6/10, for ER-Tracker, Cell-Mask, and Mito-Tracker, respectively). A reconstructed two-photon fluorescence 3-D image of HepG2 cells treated with **YP2** provided further evidence that our strategy was indeed organelle-specific, enabling high-resolution imaging of phosphatase activities only in predetermined intracellular locations, and thereby minimizing interference fluorescence from other sources (Supporting Information, Figure S9). The diffusion problem encountered by most other small molecule imaging probes,[12] was effectively abrogated in the current study through the organelle-specific "trapping" of CPPs by their cellular interacting counterparts.[28c] Probe-treated cells, if not UV-irradiated, showed no fluorescence, indicating the temporal control of our "caging" strategy (Supporting Information, Figure S8). Cells treated with Na_3VO_5 (a general phosphatase inhibitor) showed undetectable fluorescence signals under the same imaging conditions (Figure S8). Both HeLa and HepG2 cells showed similar organelle-specific imaging results (compare Figure 6A and 6B), indicating the strategy is amenable to other mammalian cells. Both one- and two-photon fluorescence microscopy provided similar imaging results (compare Supporting Information, Figure S7 and Figure 6).[21a]

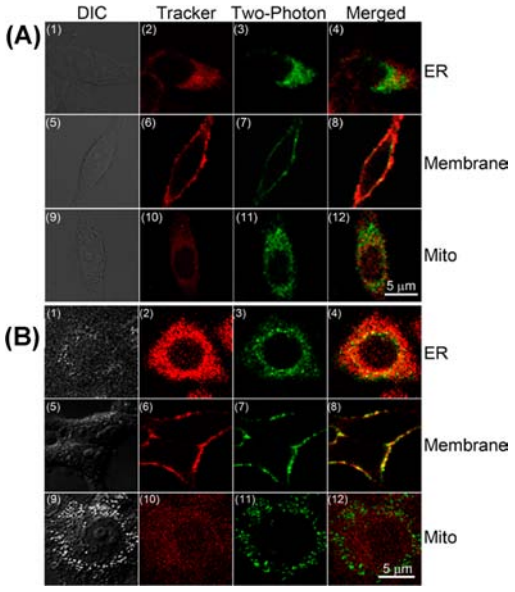

Figure 6. Two-photon fluorescence microscopy (800 nm) of endogenous phosphatase activities in live mammalian cells (A, HeLa; B, HepG2) by **YP1**/**YP2**/**YP3** probes. Live cells were incubated with the probe (8−10 μM) for 1−2 h, followed by UV irradiation (2 min) and the addition of a tracker (0.25 μg/mL), then further incubated for 30 min, before being imaged. Probes used: **YP1** in panels 1−4; **YP2** in panels 5−8; **YP3** in panels 9−12. All images were acquired in the same way. Scale bar = 5 μm.

Tumor Cell-Specific Imaging Using YP4. We next investigated whether this newly developed strategy could be extended to imaging phosphatase activities in a tumor cell-specific manner. Elevated levels of phosphatase activities are found in many cancerous cells and tissues.[2] Imaging agents that are highly responsive toward diseased cells/tissues hold great promises in diagnosis and therapeutics. Previously, Tsien and co-workers developed a tumor-targeting strategy based on selective local unleashing of CPPs.[25] Herein, we showed the successful application of this method to our newly developed imaging probes (Figure 2). Cellular uptake of **YP4**, which was conjugated to the azide-modified **P4** peptide, by normal mammalian cells was not expected due to a lack of overexpressed MMPs on their cell surface. In our imaging experiments with **YP4** and live HeLa cells (known to overexpress MMPs on the cell surface), we observed both MMP and time-dependent cellular uptake of the probe and imaging of endogenous phosphatase activities (Figure 7). A control experiment carried out in the presence of GM6001 (a general MMP inhibitor[29]) showed only moderate fluorescence signals at cell periphery after 120 min of incubation (Figure 7A), indicating nonspecific association between the uncleaved **YP4** and cell membranes, but no cellular internalization. On the contrary, HeLa cells treated with **YP4** started to develop strong fluorescence signals on the plasma membrane after 30 min (Figure 7B), indicating membrane association. After 60 min, strong fluorescence was observed both on the plasma membrane and in the cytoplasm. After 120 min, most

dx.doi.org/10.1021/ja3036256 | J. Am. Chem. Soc. 2012, 134, 12157−12167

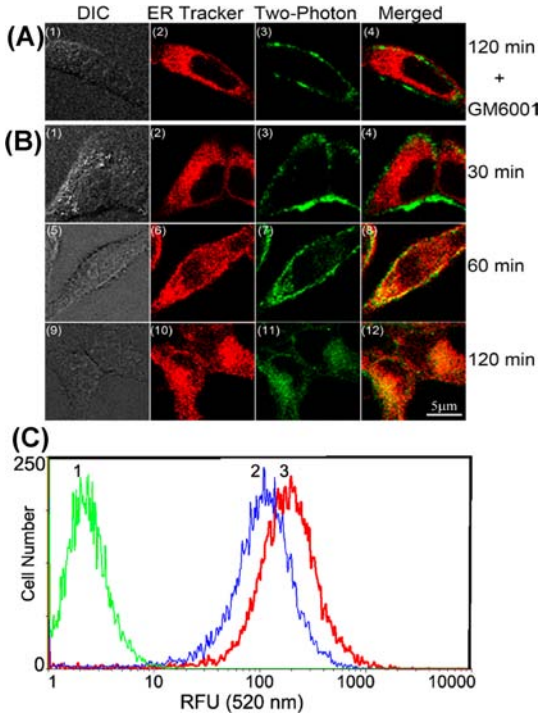

Figure 7. (A,B) TPFM (800 nm) of endogenous phosphatase activities in live HeLa cells treated with the tumor-specific probe, **YP4**. (A) **YP4** + HeLa cells + GM6001 (500 nM). Images were taken after 120 min of incubation. (B) **YP4** + HeLa cells. Images were taken after incubation for 30 min (panels 1–4), 60 min (panels 5–8), and 120 min (panels 9–12). Tracker channel: ER-Tracker (0.25 μg/mL). Scale bar = 5 μm. (C) Flow cytometry analysis of HeLa cells incubated with **YP4** (120 min), followed by UV irradiation and FACS analysis: (1) untreated cells; (2) cells incubated with **YP4** in the presence of GM6001 (500 nM); (3) cells incubated with **YP4** only.

fluorescence signals were detected in the ER, indicating complete internalization of the probe and successful detection of subcellular phosphatase activities. Similar results were obtained with a flow cytometry experiment (Figure 7C), where at least 2- to 3-fold increase in fluorescence was detected from HeLa cells treated with **YP4** versus those treated with **YP4** plus GM6001 (Figure 7C).

Two-Photon Imaging of Animal Tissues. As earlier discussed, two-photon fluorescence microscopy is particularly useful for imaging deep tissues and animals, owing to its increased penetration depth and other key advantages.[9,20,21] Despite recent advances in the development of 2P small molecule probes, few of them have been successfully designed to image endogenous enzymatic activities.[17,20,21] Our long-standing research interests in Catalomics has prompted us to start looking into enzyme-detecting, small molecule probes that can work in live tissues and animals.[30] In the current study, we have successfully imaged endogenous phosphatase activities deep inside animal tissues using our probes (Figure 8). The fresh brain of one day-old female Drosophila was dissected and incubated with 20 μM of either **Y2** or uncaged **YP2** for 6 h at room temperature. Subsequently, TPFM images of the tissues were taken at a depth of ~110 μm (Figure 8); the results revealed distribution of endogenous phosphatase activities mostly in the medulla region of the tissue (panels 2 and 5). Na_3VO_5-treated tissues shows undetectable fluorescence signals under similar imaging conditions (insets in panel 2). Control experiments were carried out with tissues treated with the ELF

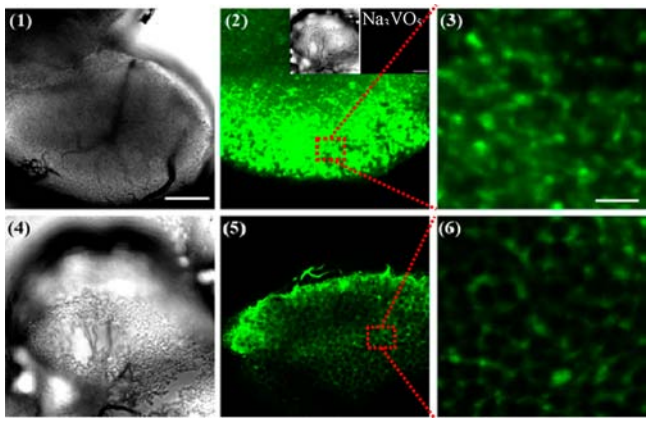

Figure 8. 2P imaging of endogenous phosphatase activities in fresh brains of one day old live female Drosophila using **Y2** and uncaged **YP2**. The images were taken at 800 nm with 40× magnification. Drosophila brains were incubated with the probes (20 μM) for 6 h. Probes used: **Y2** in panels 1–3; uncaged **YP2** in panels 4–6. (1,4) Bright-field images of half brain. (2,5) TPEF images of medulla region; insets are images obtained from the brain treated with Na_3VO_5 (100 μM) 30 min prior to incubation with **Y2**; (3,6) Enlarged images of the red boxes in panels 2 and 5 at a depth of ~110 μm with 40× magnification. Scale bar: (1,4, and insets) 150 μm; (3,6) 20 μm.

97 detection kit, which was shown to detect fluorescence signals of the tissues only at a depth of up to 35 μm (Supporting Information, Figure S10). This much deeper penetration, coupled with the significantly lower background fluorescence and better clarity observed in our TPFM images, clearly demonstrated the potential application of these newly developed, two-photon probes for tissue-based imaging experiments in future.

CONCLUSION

A novel two-photon dye, 2-hydroxy-4,6-bis(4-hydroxystyryl)-pyrimidine (**Y1**), based on a previously reported dye, 2-hydroxy-4,6-bis(4-(diethylamino)styryl)pyrimidine,[19] was disclosed for the first time. A significant advance in our current study is the finding that the highly fluorescent **Y1**, upon attachment of electron-withdrawing phosphate groups to its phenolic moieties (to make **Y2**), could be rendered only weakly fluorescent. This thus makes the **Y1**/**Y2** system the first fluorogenic, two-photon pair capable of real-time detection of phosphatase activities. Other existing small molecule phosphatase reporters based on common one-photon dyes including DiFMUP, FDP, and ELF 97 are not ideal for robust two-photon imaging applications, as they are made of one-photon dyes such as coumarin and fluorescein which have undesirable 2P photophysical properties. Despite having two phosphate groups in **Y2**, we found the monodephosphorylation step (k_1) was the rate-determining step, with the second dephosphorylation step (k_2) calculated to be ~4× faster. In fact, we were not able to detect the presence of the monodephosphorylated intermediate **Y5** throughout the **Y2**→**Y1** process. This indicates the overall fluorescence release from the **Y2**→**Y1** conversion in our reporter system could be used to directly follow endogenous phosphatase activities in real time. We have subsequently conjugated **Y3** (the caged version of **Y2**) to different cell-penetrating peptides. The resulting probes **YP1**–**YP4** were successfully used as imaging probes to detect endogenous phosphatase activities in both live mammalian cells and Drosophila brains. We showed that with the aid of CPPs,

dx.doi.org/10.1021/ja3036256 | J. Am. Chem. Soc. 2012, 134, 12157–12167

our probes could be effectively delivered to cells in an organelle- and tumor cell-specific manner. Diffusion problems normally associated with small molecule imaging probes were abrogated. We found our probes could image endogenous phosphatase activities in Drosophila brains at a depth of >100 μm. Further work will focus on the extension of this novel strategy to the imaging of other classes of enzymes.[31] One of the most obvious drawbacks about our current strategy is that the probes at present are not able to distinguish different classes of phosphatases. In fact, imaging results obtained from this study, including those in mammalian cells and Drosophila brains, likely came from cumulative enzymatic activities of different endogenous phosphatases, e.g. protein phosphatases, acidic and alkaline phosphatases that were present at the specific organelle during the time of the experiment. We are however enthusiastic that, in future, class- and substrate-specific small molecule probes of phosphatases may be discovered.[6,32]

EXPERIMENTAL SECTION

General Information. All chemicals were purchased from commercial vendors and used without further purification, unless otherwise noted. *N*,*N*-Dimethylformamide (DMF) and dichloromethane (DCM) were distilled over CaH_2. All nonaqueous reactions were carried out under a nitrogen/argon atmosphere in oven-dried glasswares. ^{1}H NMR, ^{31}P NMR, and ^{13}C NMR spectra were recorded on a Bruker model Avance 300 MHz or DPX-500 MHz NMR spectrometer. Chemical shifts are reported in parts per million relative to internal standard tetramethylsilane ($Si(CH_3)_4$ = 0.00 ppm) or residual solvent peaks ($CDCl_3$ = 7.26 ppm, DMSO-d_6 = 2.50 ppm, MeOD = 3.31 ppm). ^{1}H NMR coupling constants (J) are reported in Hertz (Hz) and multiplicity is indicated as follows: s (singlet), d (doublet), t (triplet), q (quartet), m (multiplet), br s (broad singlet), br d (broad doublet), dd (doublet of doublet), dt (doublet of triplet), dq (doublet of quartet), tq (triplet of quartet). The chemical shift of ^{31}P NMR is reported relative to H_3PO_4 = 0.00 ppm. Analytical HPLC and mass spectra were recorded on a Shimadzu LC-IT-TOF or LC-ESI system equipped with an autosampler, using reverse-phase Phenomenex Luna 5 μm C_{18} 100 Å 50 × 3.0 mm columns. Preparative HPLC was carried out on a Gilson preparative HPLC system using Trilution software and a reverse-phase Phenomenex Luna 5 μm $C_{18(2)}$ 100 Å 50 × 30.00 mm column. 0.1% TFA/H_2O and 0.1% TFA/acetonitrile were used as eluents. The flow rate was 0.6 mL/min for analytical HPLC and 10 mL/min for preparative HPLC. UV−vis absorption and fluorescence spectra were measured by using a Shimadzu UV−vis spectrophotometer and a Perkin-Elmer LS50 spectrofluorometer, respectively. The two-photon excited fluorescence measurements were performed by using a Spectra Physics femtosecond Ti:sapphire oscillator (Tsunami) as the excitation source. The output laser pulses have a tunable center wavelength from 750 to 860 nm with pulse duration of 40 fs and a repetition rate of 76 MHz. The laser beam was focused onto the samples that were contained in a cuvette with a path length of 1 cm. The emission from the samples was collected at 90° angle by a pair of lenses and an optical fiber that was connected to a monochromator (Acton, Spectra Pro 2300i) coupled with CCD (Princeton Instruments, Pixis 100B) system. A short pass filter with a cutoff wavelength at 700 nm was placed before the spectrometer to minimize the scattering from the pump beam. All the measurements were performed at room temperature. Cell-permeability assay was carried out, as previously described,[33] with MDCK (Madin-Darby canine kidney) cells and with caffeine and lucifer yellow as controls. All images were acquired on Leica TCS SP5X confocal microscope system equipped with Leica HCX PL APO 63x/1.20 W CORR CS, 405 nm diode laser, argon ion laser, white laser (470 to 670 nm, with 1 nm increments, with 8 channels AOTF for simultaneous control of 8 laser lines, each excitation wavelength provides 1.5 mV), an PMT detector ranging from 420 to 700 nm for steady state fluorescence, and Ti-Sapphire laser (~4 W at 800 nm), the PMT detector ranged from 420 to 700 nm for steady state fluorescence and nondescanned detectors (NDD) for the two-photon excited fluorescence, immediately. Images were processed with Leica Application Suite Advanced Fluorescence (LAS AF). Flow cytometry analysis was performed on a BD LSR II bioanalyzer equipped with a 350 nm UV air-cooled laser. The data was analyzed using BD FACSDiva software.

Chemical Synthesis. The overall synthetic scheme was provided as Scheme S1 in the Supporting Information.

*Diethyl 4-Formylphenyl Phosphate (**2**).* 4-Hydroxybenzaldehyde (0.24 g, 2 mmol) was dissolved in dry DCM (10 mL), followed by the addition of DMAP (0.03 g, 0.25 mmol), and the mixture was stirred at room temperature for 10 min, then cooled on an ice bath. Subsequently, diethyl phosphorochloridate (0.52 g, 3 mmol) in 10 mL of dry DCM was added dropwise to the mixture, followed by addition of triethylamine (0.7 mL, 5 mmol). The reaction was stirred on the ice bath for 2 h, then at room temperature for another 8 h. The reaction mixture was concentrated and purified by flash chromatography to afford **2** as light yellow oil (0.31 g; 60% yield). ^{1}H NMR (300 MHz, $CDCl_3$) δ 1.37 (dt, J_1 = 6.9 Hz, J_2 = 1.2 Hz, 6H), 4.27 (m, 4H), 7.41 (d, J = 8.7 Hz, 2H), 7.90 (d, J = 8.7 Hz, 2H), 9.97 (s, 1H). ^{13}C NMR (75 MHz, $CDCl_3$) δ 15.64, 15.73, 64.58, 64.66, 120.16, 120.23, 131.27, 133.02, 155.04, 155.12, 190.34. ^{31}P NMR (121 MHz, $CDCl_3$) δ −6.67.

*4-Aldehydephenyl Bis(2-nitrobenzyl) Phosphate (**3**).* The compound bis(2-nitrobenzyl)hydrogen phosphate was synthesized according to reported procedures (63% yield).[34] ^{1}H NMR (300 MHz, MeOD) δ 8.08 (d, 2H), 7.69−7.78 (m, 4H), 7.54 (t, J = 9.0 Hz, 2H), 5.43 (d, J = 3.8 Hz, 4H). ^{13}C NMR (75 MHz, MeOD) δ 166.60, 148.50, 135.11, 130.13, 129.76, 125.87. ^{31}P NMR (121 MHz, MeOD) δ −0.71. After adding bis(2-nitrobenzyl)hydrogen phosphate (5.5 g, 15 mmol) into dry DCM, oxalyl chloride (6.5 mL, 75 mmol) was added with catalytic amount of DMF to initiate the reaction. The reaction solution was stirred at room temperature for 2 h. The solvent and oxalyl chloride were removed *in vacuo* to give a light yellow oil. Next, 4-hydroxybenzaldehyde (0.61 g, 5 mmol) was dissolved in dry DCM (20 mL), followed by the addition of DMAP (0.06 g, 0.5 mmol), and the mixture was stirred at room temperature for 10 min. Then the light yellow oil (now redissolved in 10 mL dry DCM) was added dropwise to the mixture on an ice bath, followed by addition of triethylamine (1.4 mL, 10 mmol). The reaction was left on ice for 2 h, and then warmed to room temperature for another 8 h. The reaction mixture was concentrated and purified by flash chromatography to afford **3** as a light yellow oil (1.2 g; 51% yield). ^{1}H NMR (300 MHz, $CDCl_3$) δ 5.21 (d, J = 7.8 Hz, 4H), 7.44 (d, J = 8.4 Hz, 2H), 7.45 (dt, J_1 = 8.4 Hz and J_2 = 1.8 Hz, 2H), 7.65 (m, 4H), 7.82 (d, J = 8.7 Hz, 2H), 8.06 (d, J = 7.8 Hz, 2H), 9.90 (s, 1H). ^{13}C NMR (75 MHz, $CDCl_3$) δ 67.07, 67.13, 120.55, 120.62, 125.16, 128.62, 129.35, 131.36, 131.47, 131.75, 133.67, 14.23, 146.75, 154.70, 190.68. ^{31}P NMR (121 MHz, $CDCl_3$) δ −6.98. IT-TOF-MS: m/z $[M+Na]^+$ calcd, 495.07; found, 495.05.

*2-Hydroxy-4,6-bis(4-hydroxystyryl)pyrimidine (**Y1**).* **Y1** was synthesized according to reported methods.[19] A mixture of 2-hydroxy-4,6-dimethylpyrimidine hydrochloride (**1**; 0.8 g, 5 mmol) and 4-hydroxybenzaldehyde (1.34 g, 11 mmol) in 20 mL of ethanol was stirred under an N_2 atmosphere at room temperature for 1 h. Hydrochloric acid (2 mL, 3 M) was added dropwise to the reaction mixture which was then refluxed for 30 h. The solvent was removed, and the residue was washed with DCM three times. The resulting solid was purified by flash chromatography (10:1 DCM/methanol) to give **Y1** as a red powder (1.33 g; 80% yield). ^{1}H NMR (300 MHz, DMSO-d_6) δ 6.80 (d, J = 16.2 Hz, 2H), 6.82 (s, 1H), 6.85 (d, J = 8.4 Hz, 4H), 7.51 (d, J = 8.4 Hz, 4H), 7.78 (d, J = 16.2 Hz, 2H), 10.06 (s, 1H), 11.74 (s, 1H). ^{13}C NMR (75 MHz, DMSO-d_6) δ 98.90, 115.97, 119.05, 126.12, 129.70, 139.13, 156.76, 159.59, 162.01. IT-TOF-MS: m/z $[M+H]^+$ calcd, 333.12; found, 333.12.

*2-Hydroxy-4,6-bis(4-dihydrogen phosphate)pyrimidine (**Y2**).* A mixture of 2-hydroxy-4,6-dimethylpyrimidine hydrochloride (**1**; 0.08 g, 0.5 mmol) and diethyl 4-formylphenyl phosphate (0.39 g, 1.5 mmol) in 10 mL of ethanol was stirred under an Ar atmosphere at room

temperature for 1 h. Hydrochloric acid (0.2 mL, 3 M) was added dropwise to the reaction mixture which was then refluxed for 48 h. The solvent was removed, and the resulting residue was washed with ethanol (3×) then concentrated in vacuo. Twenty milliliters of DCM was subsequently added, and the resulting mixture was stirred at room temperature for 10 min before being cooled on an ice bath. TMSI (0.46 g, 2.2 mmol) was added dropwise. The reaction was stirred further for 4 h before being quenched by the addition of 10 mL of saturated ammonium chloride solution. Upon concentration in vacuo, the residue was purified by semipreparative HPLC on a C_{18} column to give **Y2** as a dark-red solid (37 mg; 15% yield). ^{1}H NMR (300 MHz, DMSO-d_6) δ 6.98 (d, J = 16.2 Hz, 2H), 7.17 (s, 1H), 7.27 (d, J = 8.4 Hz, 2H), 7.67 (d, J = 8.7 Hz, 4H), 7.97 (d, J = 16.2 Hz, 2H), 8.62 (bs, 1H). ^{31}P NMR (121 MHz, DMSO-d_6) δ −5.79. IT-TOF-MS: m/z $[M+H]^+$ calcd, 493.05; found, 493.06.

*2-Hydroxy-4,6-bis(4-bisnitrobenzyl phosphate)pyrimidine (**Y3**).* A mixture of 2-hydroxy-4,6-dimethylpyrimidine hydrochloride (**1**; 0.08 g, 0.5 mmol) and **3** (0.71 g, 1.5 mmol; prepared according to ref 34) in 10 mL of ethanol was stirred under an Ar atmosphere at room temperature for 1 h. Hydrochloric acid (0.2 mL, 3 M) was added dropwise. The reaction mixture was refluxed for 48 h. The solvent was removed *in vacuo* and the resulting residue was washed with DCM (3×). Next the solid was purified by semipreparative HPLC on a C_{18} column to give **Y3** as a dark-red solid (80 mg; 21% yield). ^{1}H NMR (300 MHz, DMSO-d_6) δ 5.32 (d, J = 7.5 Hz, 4H), 6.98 (d, J = 16.2 Hz, 2H), 7.12 (m, 2H), 7.15 (m, 3H), 7.59 (m, 6H), 7.76 (m, 4H), 8.10 (d, J = 7.8 Hz, 2H), 8.16 (d, J = 16.2 Hz, 2H). ^{31}P NMR (121 MHz, DMSO-d_6) δ −6.23. IT-TOF-MS: m/z $[M+H]^+$ calcd, 763.11; found, 763.09.

*2-Propargyloxy-4,6-bis(4-bisnitrobenzyl phosphate) Pyrimidine (**Y4**).* **Y3** (38 mg, 0.05 mmol), propargyl bromide (18 mg, 0.15 mmol) and K_2CO_3 (14 mg, 0.1 mmol) were mixed in 5 mL of dry DMF. The reaction mixture was stirred under an Ar atmosphere at 80 °C for 48 h. Upon removal of the solvent *in vacuo*, the resulting residue was purified by semipreparative HPLC on a C_{18} column to give **Y4** as a dark-red solid (15 mg; 37.5% yield). ^{1}H NMR (300 MHz, DMSO-d_6) δ 3.53 (s, 1H), 5.11 (s, 2H), 5.32 (d, J = 4.2 Hz, 4H), 7.11 (d, J = 8.4 Hz, 2H), 7.29 (m, 5H), 7.57 (br d, 6H), 7.77 (br s, 4H), 7.87 (d, J = 9.6 Hz, 2H), 8.09 (d, J = 4.5 Hz, 2H). ^{31}P NMR (121 MHz, DMSO-d_6) δ −7.72. IT-TOF-MS: m/z $[M+H]^+$ calcd, 801.13; found, 801.11.

*(E)-4-(4-Hydroxystyryl)-6-methylpyrimidin-2-ol (**4**).* A mixture of 2-hydroxy-4,6-dimethylpyrimidine hydrochloride (**1**; 0.8 g, 5 mmol) and 4-hydroxybenzaldehyde (0.67 g, 5.5 mmol) in 20 mL of ethanol was stirred under an N_2 atmosphere at room temperature for 1 h. Hydrochloric acid (2 mL, 3 M) was added dropwise to the reaction mixture which was then refluxed for 24 h. The solvent was removed, and the residue was washed with DCM three times. The resulting solid was purified by flash chromatography (10:1 DCM/methanol) to give **4** as a yellow powder (0.82 g; 72% yield). ^{1}H NMR (300 MHz, DMSO-d_6) δ 2.44 (s, 3H), 6.91 (d, J = 16.0 Hz, 1H), 6.93 (d, J = 8.5 Hz, 2H), 7.16 (s, 1H), 7.59 (d, J = 9.0 Hz, 2H), 8.19 (d, J = 16.0 Hz, 1H). ESI-MS: m/z $[M+H]^+$ calcd, 229.1; found, 229.2.

*4-((E)-2-(2-Hydroxy-6-((E)-4-hydroxystyryl)pyrimidin-4-yl)vinyl)-phenyl Dihydrogen Phosphate (**Y5**).* A mixture of **4** (0.23 g, 1 mmol) and diethyl 4-formylphenyl phosphate (**2**; 0.28 g, 1.5 mmol) in 10 mL of pyridine and 50 μL of piperidine was refluxed for 24 h. The solvent was removed, and the resulting residue was washed with ethanol (3×) and then concentrated in vacuo. Twenty milliliters of DCM was subsequently added, and the resulting mixture was stirred at room temperature for 10 min before being cooled on an ice bath. TMSI (0.46 g, 2.2 mmol) was added dropwise. The reaction was stirred further for 4 h before being quenched by the addition of 10 mL of saturated ammonium chloride solution. Upon concentration *in vacuo*, the residue was purified by semipreparative HPLC on a C_{18} column to give **Y5** as a dark-red solid (45 mg; 11% yield). ^{1}H NMR (300 MHz, DMSO-d_6) δ 6.82 (d, J = 16.2 Hz, 1H), 6.0 (d, J = 8.4 Hz, 2H), 6.95 (d, J = 16.2 Hz, 1H), 7.05 (s, 1H), 7.20 (d, J = 8.4 Hz, 2H), 7.55 (d, J = 8.4 Hz, 2H), 7.60 (d, J = 8.4 Hz, 2H), 7.82 (d, J = 16.2 Hz, 1H), 7.90 (d, J = 16.2 Hz, 1H), 9.35 (bs, 1H). ^{31}P NMR (121 MHz, DMSO-d_6) δ −5.76. ESI-MS: m/z $[M+H]^+$ calcd, 413.1; found, 413.2.

Solid-Phase Peptide Synthesis (SPPS). The peptides were synthesized on rink amide resin using Irori microkan reactors (150 mg/reactor; loading level =0.6 mmol/g), as previously described.[26] Briefly, Fmoc deprotection was carried out with piperidine (20% v/v in DMF; 1 h). The washing cycles were done with DMF (3×), DCM (3×), MeOH (3×) and DMF (1×). The resins were then added to a preactivated DMF solution containing Fmoc-protected amino acid (4 equiv), HOBt (4 equiv), HBTU (4 equiv), and DIEA (4 equiv). The coupling reaction was carried out for 12 h at room temperature with constant shaking. Complete coupling was confirmed by the Ninhydrin test. For the coupling of palmitoyl group to the first Lys residue in **P2**, Fmoc-Lys(Mtt)−OH was first coupled to the resin. Subsequently, the Mtt group on the Ω-amino group was removed with 1% TFA ((v/v) in DCM for 1 h). Upon neutralization with DIEA, to the resin was added a preactivated DMF solution containing palmitic acid (4 equiv), HOBt (4 equiv), HBTU (4 equiv), and DIEA (4 equiv). The reaction was carried out for 12 h at room temperature with constant shaking. For the capping of succinoyl group to **P4**, the *N*-terminus of **P4** was coupled with a DMF solution containing succinic anhydride (4 equiv) and DIEA (4 equiv), for 4 h at room temperature. For coupling of 4-azidobutanoic acid, the *N*-termini of **P1**, **P2**, and **P3** resin-bound peptides were treated with a preactivated DMF solution containing 4-azidobutanoic acid (4 equiv), HOBt (4 equiv), HBTU (4 equiv), and DIEA (4 equiv), for 4 h at room temperature. **P4** needed the attachment of 4-azidobutanoic acid at the Ω-amino group of the first Lys residue. Upon removal of the Mtt group on the resin-bound Fmoc-Lys(Mtt)−OH, the resin was then coupled to 4-azidobutanoic acid similarly. The peptides were cleaved from the solid support by adding a cleavage cocktail of TFA/TIS/H_2O (95/2.5/2.5) to the resins and shaking for 2 h at room temperature. Following ether precipitation and preparative HPLC, the peptides (**P1**−**P4**) were obtained as white solids. The peptides were characterized using IT-TOF LC-MS. The m/z values obtained were fractions of the mass of target peptides due to positive charges present in the peptides. **P1**: (N_3−KKKRKV−NH_2), $C_{39}H_{77}N_{17}O_7$, $[M]^+$: m/z = 895.62; LC−MS found for $[(M+2H)/2]^+$ = 448.80. **P2**: N_3−KK(palmitoyl)−NH_2), $C_{32}H_{62}N_8O_4$, $[M]^+$: m/z = 622.49; LC−MS found for $[M+H]^+$ = 623.50. **P3**: N_3−F_xrF_xK−NH_2, $C_{34}H_{62}N_{12}O_5$, $[M]^+$: m/z = 718.50; LC−MS found for $[M+H]^+$ = 719.47. **P4**: UeeeeeeeeGGPLGLAGrrrrrrrrrK(N_3)-NH_2, $C_{136}H_{234}N_{58}O_{46}$, $[M]^+$: m/z = 3415.78; LC-MS found for $[(M+3H)/3]^+$ = 1139.92, $[(M+4H)/4]^+$ = 855.44.

Click Assembly of YP1−YP4. For the synthesis of **YP1**/**YP2**/**YP3**, 4 μL of each peptide (20 mM stock), 8 μL of **Y4**, 8 μL of $CuSO_4{\cdot}5H_2O$ (4 mM stock) and 8 μL of *tris*-[benzyltriazolylmethyl]-amine (TBTA) (10 mM stock) were added to 48 μL of DMSO/H_2O (1:1). The resulting solution was mixed, followed by addition of sodium ascorbate (4 μL in 50 mM stock). The tubes were capped and shaken at room temperature for 2 days. For **YP4** synthesis, 32 μL of **P4** (20 mM stock), 8 μL of **Y4** (20 mM stock), 16 μL of CuI (4 mM stock), and DIEA (10 mM stock) were added to 48 μL of DMSO/CH_3CN/H_2O (4:4:1). The tubes were capped and shaken for 24 h. The products were purified by semipreparatory HPLC and characterized by LC-MS. **YP1**: $C_{76}H_{107}N_{21}O_{20}P_2$, $[M]^+$: m/z = 1695.75; LC−MS found for $[(M+2H)/2]^+$ = 848.85. **YP2**: $C_{69}H_{92}N_{12}O_{17}P_2$, $[M]^+$: m/z = 1422.62; LC−MS found for $[(M+2H)/2]^+$ = 712.29. **YP3**: $C_{71}H_{92}N_{16}O_{18}P_2$, $[M]^+$: m/z = 1518.63; LC−MS found for $[(M+2H)/2]^+$ = 760.26. **YP4**: $C_{173}H_{264}N_{62}O_{59}P_2$, $[M]^+$: m/z = 4215.90; LC−MS found for $[(M+3H)/3]^+$ = 1406.93, $[(M+4H)/4]^+$ = 1055.45.

Photo Cleavage Assay. The caged phosphate groups of **Y3** were introduced to temporally control the detection of endogenous phosphatase activities *via* an UV-mediated uncaging reaction. It was established that completely uncaged product (**Y2**) could be obtained from **Y3** ($C = 1.6 \times 10^{-6}$ mol L^{-1}) under conditions of 500 $\mu J/cm^2$ UV exposure (at 400 nm) for 2−5 min at room temperature.

In vitro Phosphatase Assay. The expression and purification of PTP1B were previously reported.[35] Alkaline phosphatase was purchased from Sigma (USA). PP1 and PP2B (2500 U/mL) were obtained from NEB (USA). PTP1B were prepared to ∼0.2 μg/μL in

Hepes buffer (1×, pH = 7.5, supplemented with 0.05 M NaCl, 2.5 mM EDTA, 2 mM DTT, and 0.02 or 0.08% Triton X-100). The experiment for testing PTP1B activities was as the following: PTP1B (~2 μg) was incubated with either **Y3** or **Y2** (1.6 μM final concentration) in 1 mL of Hepes buffer. For the experiment involving **Y3**, the reaction mixture was first irradiated with 500 μJ/cm^2 UV exposure (at 400 nm) for 5 min at room temperature, as above-described, prior to the addition of PTP1B. The dephosphorylation reaction was closely monitored by both LC–MS and either a Perkin-Elmer LS50 spectrofluorometer (Figure 4C) or an in-house two-photon spectrometer. The reaction rate constant was defined from the half-life equation for a second-order reaction dependent on one second-order reactant ($k = t_{1/2}^{-1}\,[A]_0^{-1}$). Experiments with **Y5** were similarly carried out (Figure 4D).

For photostability experiments of **Y1** and three commercial dyes in Hepes buffer (Figure 3A), fluorescence intensities were collected at 550 nm for **Y1**, 450 nm for courmarin, 520 nm for HPQ, and 520 nm for fluorescein with 60 s intervals using an excitation wavelength 405 nm for **Y1**, 350 nm for courmarin, 350 nm for HPQ, and 488 nm for fluorescein, respectively. For the pH effect on the one-photon excited fluorescence intensity of **Y1** at room temperature (Figure 3B), the fluorescence intensity was collected at 550 nm (λ_{ex} = 405 nm) with 1.0 μM of the probe prepared in Hepes buffers having different pH values.

General Procedures for 1P and 2P Fluorescence Imaging. Both HeLa and HepG2 cell lines used in our imaging experiments were cultured in growth media (DMEM) supplemented with 10% fetal bovine serum, 100.0 mg/L streptomycin, and 100 IU/mL penicillin. Cells were maintained in a humidified atmosphere of 5% CO_2 at 37 °C to a confluency of around 80%. Tissues used in our imaging experiments were fresh brains of one day-old live female Drosophila. All the trackers were from Invitrogen (Ex = 590 nm for ER-Tracker Red glibenclamide BODIPY TR (PMT range: 600–650 nm), Ex = 554 nm for MitoTracker Red CMXRos dye (PMT range: 570–650 nm), and Ex = 543 nm for CellMask Plasma Membrane Stains C10045 (PMT range: 555–650 nm)).

For time-dependent one-photon excited fluorescence imaging of HepG2 cells treated with **Y3** (Figure 5), cells were added to **Y3** (10 μM) and UV-irradiated for 2 min. Images were collected at 460–550 nm with 60 s intervals using an excitation wavelength at 405 nm. For control experiments with the four dye-CPP conjugates (Supporting Information, Figure S6), HeLa cells were added to the tested peptide followed by further incubation (1 μM for SG-KKKRKV × 2 h, SG-F_xrF_xK × 1 h, SG-RRRRRRRRR × 2 h, and 0.5 μM for SG-KK(palmitoyl) × 30 min). Subsequently, cells were treated with 0.25 μg/mL of the corresponding organelle tracker following protocols provided by the vendor and washed three times with PBS before being imaged.

The ELF 97 Endogenous Phosphatase Detection Kit (Invitrogen, E6601) was used, in control experiments, to endogenous phosphatase activities in fixed mammalian cells and Drosophila brains. Mammalian cells were seeded on glass-bottom dishes (Mattek) and grown until 70–80% confluency. The growth medium was removed; the cells were first fixed with 3.7% paraformaldehyde in PBS for 10 min and washed three times with PBS. The cells were incubated with 0.25 μg/mL of the corresponding organelle tracker. Next, the fixed cells were incubated with 1 × ELF 97 in detection buffer and imaged (Supporting Information, Figure S4).

Live-Cell Imaging with Organelle-Specific Probes. Four probe-peptide conjugates (**YP1** to **YP4**) were used to image endogenous phosphatase activities in live HeLa and HepG2 cells. Cells were seeded in glass-bottom dishes (Mattek) and grown until 70–80% confluency. Subsequently, the cells were incubated with the peptide (10 μM for **YP1**, **YP3**, and **YP4**, 8 μM for **YP2**; prepared in fresh media). Upon further incubation (2 h for **YP1** and **YP4**, 1 h for **YP2** and **YP3**), cells were UV irradiated (2 min) then further incubated with 0.25 μg/mL of the organelle tracker. Next, cells were washed three times with PBS before and immediately imaged with Leica TCS SP5X Confocal Microscope System. Meanwhile, another identical set of samples was similarly treated as described above and without UV-irradiated for negative control. All the cells were then treated for further incubation at 37 °C and washed three times with PBS and imaged. For the inhibition experiment in tumor cell-specific imaging with **YP4**, the cells were first incubated with GM6001 (500 nM, Millipore) for 30 min, before being treated by the probe and imaged as above-described. Flow cytometry experiments were done as previously reported.[18b] HeLa cells were seeded in Nunc 3.5 cm dishes (cat. no. 153066) and grown until ~90% confluency. Two sets of cells were prepared with or without first being incubated with GM6001 (500 nM, Millipore) for 30 min, before being treated by 10 μM of **YP4** (prepared in fresh media). DMSO was used as negative control. Upon further incubation for 2 h, cells were UV irradiated (2 min) and further incubated for 0.5 h, then washed with PBS (2×), detached from dishes, washed (with PBS), fixed with 3.8% paraformaldehyde in PBS for 10 min, and then analyzed by FACS (Figure 7C).

Imaging of Drosophila Brains. Brains were prepared from a one day-old female Drosophila. Brains were incubated with ELF97 (0.5 h), **Y2** (6 h), and uncaged **YP2** (6 h) in DMEM under a humidified atmosphere of 5:95 (v/v) of CO_2/air at 37 °C. For inhibition experiments, the cells were incubated with Na_3VO_5 (100 μM) 30 min prior to incubation with **Y2**. Treated brains were subsequently washed three times with PBS and transferred to poly-L-lysine-coated coverslips, and imaged. The images were taken at ~35 μm (for ELF 97; see Supporting Information, Figure S10) and ~110 μm (for all other experiments) by changing the *Z*-axis thickness.

■ ASSOCIATED CONTENT

Ⓢ Supporting Information

Other relevant experimental sections, spectral characterization of new compounds, and supplementary biological results. This material is available free of charge via the Internet at http://pubs.acs.org.

■ AUTHOR INFORMATION

Corresponding Author

chmyaosq@nus.edu.sg

Notes

The authors declare no competing financial interest.

■ ACKNOWLEDGMENTS

Financial support was provided by the Agency for Science, Technology and Research (R-143-000-391-305) and the Ministry of Education (R-143-000-394-112). We also acknowledge Madam Tong Yan in the Department of Biological Sciences (NUS) for her technical support on two-photon microscopy and Dr Lim Kah Leong (NUS) for the generous donation of the Drosophila brains.

■ REFERENCES

(1) (a) Tonks, N. K. *Nat. Rev. Mol. Cell Biol.* **2006**, *7*, 833–846. (b) Shi, Y. *Cell* **2009**, *139*, 468–484. (c) Barford, D.; Das, A. K.; Egloff, Annu. M. P. *Rev. Biophy. Biomol. Struct.* **1998**, *27*, 133–164.

(2) Östman, A.; Hellberg, C.; Böhmer, F. D. *Nat. Rev. Cancer* **2006**, *6*, 307–320.

(3) Taira, A.; Merrick, G.; Wallner, K.; Dattoli, M. *Oncology* **2007**, *21*, 1003–1010.

(4) (a) Fraser, W. D. *Curr. Opin. Rheumatol.* **1997**, *9*, 347–354. (b) Lange, P. H.; Millan, J. L.; Stigbrand, T.; Vessella, R. L.; Ruoslahti, E.; Fishman, W. H. *Cancer Res.* **1982**, *42*, 3244–3247.

(5) (a) Zhang, Z. Y. *Annu. Rev. Pharmacol. Toxicol.* **2002**, *42*, 209–234. (b) McConnell, J. L.; Wadzinski, B. E. *Mol. Pharmacol.* **2009**, *75*, 1249–1261. (c) Vintonyak, V. V.; Antonchick, A. P.; Rauh, D.; Waldmann, H. *Curr. Opin. Chem. Biol.* **2009**, *13*, 272–283.

(6) (a) Liu, S.; Zhou, B.; Yang, H. H.; He, Y.; Jiang, Z. X.; Kumar, S.; Wu, L.; Zhang, Z. Y. *J. Am. Chem. Soc.* **2008**, *130*, 8251–8260. (b) Kalesh, K. A.; Tan, L. P.; Liu, K.; Gao, L.; Wang, J.; Yao, S. Q. *Chem. Commun.* **2010**, *46*, 589–591.

(7) Yudushkin, I. A.; Schleifenbaum, A.; Kinkhabwala, A.; Neel, B. G.; Schultz, C.; Bastiaens, P. I. H. *Science* **2007**, *315*, 115−119.
(8) Newman, R. H.; Zhang, J. *Mol. Biosyst.* **2008**, *4*, 496−501.
(9) Helmchen, F.; Denk, W. *Nat. Methods* **2005**, *2*, 932−940.
(10) For recent reviews, see: (a) Edgington, L. E.; Verdoes, M.; Bogyo, M. *Curr. Opin. Chem. Biol.* **2011**, *15*, 798−805. (b) Wysockia, L. M.; Lavis, L. D. *Curr. Opin. Chem. Biol.* **2011**, *15*, 752−759. (c) Domaille, D. W.; Que, E. L.; Chang, C. J. *Nat. Chem. Biol.* **2008**, *4*, 168−175. (d) Razgulin, A.; Ma, N.; Rao, J. *Chem. Soc. Rev.* **2011**, *40*, 4186−4216. (e) Kikuchi, K. *Chem. Soc. Rev.* **2010**, *39*, 2148−2053.
(11) Tsien, R. Y. *Angew. Chem., Int. Ed.* **2009**, *48*, 5612−5626.
(12) Baruch, A.; Jeffery, D. A.; Bogyo, M. *Trends Cell Biol.* **2004**, *14*, 29−35 and references cited therein.
(13) (a) For commercially available, small-molecule phosphatase probes, see www.introgen.com. (b) Kawanishi, Y.; Kikuchi, K.; Takakusa, H.; Mizukami, S.; Urano, Y.; Higuchi, T.; Nagano, T. *Angew. Chem., Int. Ed.* **2000**, *39*, 3438−3441.
(14) Wang, Q.; Scheigetz, J.; Roy, B.; Ramachandran, C.; Gresser, M. J. *Biochim. Biophys. Acta, Proteins Proteom.* **2002**, *1601*, 19−29.
(15) Gade1, T. P.; Motley, M. W.; Beattie, B. J.; Bhakta, R.; Boskey, A. L.; Koutcher, J. A.; Mayer-Kuckuk, P. *PLoS One* **2011**, *6*, e22608.
(16) (a) Blum, G.; Mullins, S. R.; Keren, K.; Fonovic, M.; Jedeszko, C.; Rice, M. J.; Sloane, B. F.; Bogyo, M. *Nat. Chem. Biol.* **2005**, *1*, 203−209. (b) Blum, G.; von Degenfeld, G.; Merchant, M. J.; Blau, H. M.; Bogyo, M. *Nat. Chem. Biol.* **2007**, *3*, 668−677. (c) Blum, G.; Weimer, R. M.; Edgington, L. E.; Adams, W.; Bogyo, M. *PLoS One* **2009**, *4*, e6374.
(17) Hu, M.; Li, L.; Wu, H.; Su, Y.; Yang, P. -Y.; Uttamchandani, M.; Xu, Q. H.; Yao, S. Q. *J. Am. Chem. Soc.* **2011**, *133*, 12009−12020.
(18) (a) Kwan, D. H.; Chen, H. M.; Ratananikom, K.; Hancock, S. M.; Watanabe, Y.; Kongsaeree, P. T.; Samuels, A. L.; Withers, S. G. *Angew. Chem., Int. Ed.* **2011**, *50*, 300−303. (b) Ge, J.; Li, L.; Yao, S. Q. *Chem. Commun.* **2011**, *47*, 10939−10941.
(19) Li, L.; Tian, Y. P.; Yang, J. X.; Sun, P. P.; Kong, L.; Wu, J. Y.; Zhou., H. P.; Zhang, S. Y.; Jin, B. K.; Tao, X. T.; Jiang, M. H. *Chem. Commun.* **2010**, *46*, 1673−1675.
(20) For recent reviews, see: (a) Pawlicki, M.; Collins, H. A.; Denning, R. G.; Anderson, H. L. *Angew. Chem., Int. Ed.* **2009**, *48*, 3244−3266. (b) Kim, H. M.; Cho, B. R. *Chem. Commun.* **2009**, 153−164.
(21) (a) Kim, H. J.; Han, J. H.; Kim, M. K.; Lim, C. S.; Kim, H. M.; Cho, B. R. *Angew. Chem., Int. Ed.* **2010**, *49*, 6786−6789 and references cited therein. (b) Reeve, J. E.; Collins, H. A.; Mey, K. D.; Kohl, M. M.; Thorley, K. J.; Paulsen, O.; Clays, K.; Anderson, H. L. *J. Am. Chem. Soc.* **2009**, *131*, 2758−2759. (c) Kohl, T.; Heinze, K. G.; Kuhlemann, R.; Koltermann, A.; Schwille, P. *Proc. Natl. Acad. Sci. U.S.A.* **2002**, *99*, 12161−12166. (d) Botchway, S. W.; Charnley, M.; Haycock, J. W.; Parker, A. W.; Rochester, D. L.; Weinstein, J. A.; Williams, J. A. G. *Proc. Natl. Acad. Sci. U.S.A.* **2008**, *105*, 16071−16076. (e) Neveu, P.; Aujard, I.; Benbrahim, C.; Le Saux, T.; Allemand, J. -F.; Vriz, S.; Bensimon, D.; Jullien, L. *Angew. Chem., Int. Ed.* **2008**, *47*, 3744−3746. (f) Zhu, Y.; Pavlos, C. M.; Toscano, J. P.; Dore, T. M. *J. Am. Chem. Soc.* **2006**, *128*, 4267−4276. (g) Pond, S. J. K.; Tsutsumi, O.; Rumi, M.; Kwon, O.; Zojer, E.; Brédas, J. L.; Marder, S. R.; Perry, J. W. *J. Am. Chem. Soc.* **2004**, *126*, 9291−9306. (h) Feng, X. J.; Wu, P. L.; Bolze, F.; Leung, H. W. C.; Li, K. F.; Mak, N. K.; Kwong, D. W. J.; Nicoud, J. F.; Cheah, K. W.; Wong, M. S. *Org. Lett.* **2010**, *12*, 2194−2197. (i) Kim, M. K.; Lim, C. S.; Hong, J. T.; Han, J. H.; Jang, H. -Y.; Kim, H. M.; Cho, B. R. *Angew. Chem., Int. Ed.* **2010**, *49*, 364−367.
(22) (a) Rotman, B.; Zderic, J. A.; Edelstein, M. *Proc. Natl. Acad. Sci. U.S.A.* **1963**, *50*, 1−6. (b) Gee, K. R.; Sun, W. C.; Bhalgat, M. K.; Upson, R. H.; Klaubert, D. H.; Latham, K. A.; Haugland, R. P. *Anal. Biochem.* **1999**, *273*, 41−48. (c) Lavis, L. D.; Raines, R. T. *ACS Chem. Biol.* **2008**, *3*, 142−155.
(23) (a) Kolb, H. C.; Sharpless, K. B. *Drug Discovery Today* **2003**, *8*, 1128−1137. (b) Meldal, M. M.; Tornøe, C. W. *Chem. Rev.* **2008**, *108*, 2952−3015. (c) Kalesh, K. A.; Shi, H.; Ge, J.; Yao, S. Q. *Org. Biomol. Chem.* **2010**, *8*, 1749−1762.
(24) (a) Pouton, C. W.; Wagstaff, K. M.; Roth, D. M.; Moseley, G. W.; Jans, D. A. *Adv. Drug Delivery Rev.* **2007**, *59*, 698−717. (b) Resh, M. D. *Cell. Signalling* **1996**, *8*, 403−412. (c) Stewart, K. M.; Horton, K. L.; Kelley, S. O. *Org. Biomol. Chem.* **2008**, *6*, 2242−2255.
(25) Jiang, T.; Olson, E. S.; Nguyen, Q. T.; Roy, M.; Jennings, P. A.; Tsien, R. Y. *Proc. Natl. Acad. Sci. U.S.A.* **2004**, *101*, 17867−17872.
(26) (a) Loh, Y.; Shi, H.; Hu, M.; Yao, S. Q. *Chem. Commun.* **2010**, *46*, 8407−8409. (b) Li, J.; Yao, S. Q. *Org. Lett.* **2009**, *11*, 405−408. (c) Wu, H.; Ge, J.; Yang, P. -Y..; Wang, J.; Uttamchandani, M.; Yao, S. Q. *J. Am. Chem. Soc.* **2011**, *133*, 1946−1954.
(27) (a) Johnson, T. O.; Ermolieff, J.; Jirousek, M. R. *Nat. Rev. Drug Discovery* **2002**, *1*, 696−709. (b) Tournebize, R.; Andersen, S. S.; Verde, F.; Dorée, M.; Karsenti, E.; Hyman, A. A. *EMBO J.* **1997**, *16*, 5537−5549. (c) Yamashita, M.; Katsumata, M.; Iwashima, M.; Kimura, M.; Shimizu, C.; Kamata, T.; Shin, T.; Seki, N.; Suzuki, S.; Taniguchi, M.; Nakayama, T. *J. Exp. Med.* **2000**, *191*, 1869−1879.
(28) (a) Hillaert, U.; Verdoes, M.; Florea, B. I.; Saragliadis, A.; Habets, K. L. L.; Kuiper, J.; Van Calenbergh, S.; Ossendorp, F.; van der Marel, G. A.; Driessen, C.; Overkleeft, H. S. *Angew. Chem., Int. Ed.* **2009**, *48*, 1629−1632. (b) Dickinson, B. C.; Chang, C. J. *J. Am. Chem. Soc.* **2008**, *130*, 9638−9639. (c) Srikun, D.; Albers, A. E.; Nam, C. I.; Iavaron, A. T.; Chang, C. J. *J. Am. Chem. Soc.* **2010**, *132*, 4455−4465.
(29) Uttamchandani, M.; Wang, J.; Li, J.; Hu, M.; Sun, H.; Chen, K. Y. -T.; Liu, K.; Yao, S. Q. *J. Am. Chem. Soc.* **2007**, *129*, 7848−7858.
(30) (a) Uttamchandani, M.; Lu, C. H. S.; Yao, S. Q. *Acc. Chem. Res.* **2009**, *42*, 1183−1192. (b) Zhang, C. -J.; Li, L.; Chen, G. Y. J.; Xu, Q. -H.; Yao, S. Q. *Org. Lett.* **2011**, *13*, 4160−4163.
(31) (a) Yang, P. -Y.; Wang, M.; He, C. Y.; Yao, S. Q. *Chem. Commun.* **2012**, *48*, 835−837. (b) Shi, H.; Zhang, C.; Chen, G. Y. J.; Yao, S. Q. *J. Am. Chem. Soc.* **2012**, *134*, 3001−3014. (c) Shi, H.; Uttamchandani, M.; Yao, S. Q. *Chem. -Asian. J.* **2011**, *6*, 2803−2815. (d) Yang, P. -Y.; Liu, K.; Ngai, M. H.; Lear, M. J.; Wenk, M. R.; Yao, S. Q. *J. Am. Chem. Soc.* **2010**, *132*, 656−666. (e) Uttamchandani, M.; Lee, W. L.; Wang, J.; Yao, S. Q. *J. Am. Chem. Soc.* **2007**, *129*, 13110−13117.
(32) Lu, C. H. S.; Liu, K.; Tan, L. P.; Yao, S. Q. *Chem.—Eur. J.* **2012**, *18*, 28−39.
(33) Wu, H.; Ge, J.; Yao, S. Q. *Angew. Chem., Int. Ed.* **2010**, *49*, 6528−6532.
(34) Rubinstein, M.; Ptchornik, A. *Tetrahedron* **1975**, *31*, 2107−2110.
(35) (a) Srinivasan, R.; Tan, L. P.; Wu, H.; Yao, S. Q. *Org. Lett.* **2008**, *10*, 2295−2298. (b) Sun, H.; Lu, C. H. S.; Uttamchandani, M.; Xia, Y.; Liou, Y. C.; Yao, S. Q. *Angew. Chem., Int. Ed.* **2008**, *47*, 1698−1702.